THE JOURNAL OF PHYSICAL CHEMISTRY C

Article

pubs.acs.org/JPCC

Structure Prediction of Atoms Adsorbed on Two-Dimensional Layer Materials: Method and Applications

Bo Gao,[†] Xuecheng Shao,[†] Jian Lv,[‡] Yanchao Wang,*[,†] and Yanming Ma*[,†]

[†]State Key Laboratory of Superhard Materials, Jilin University, Changchun 130012, China

[‡]Beijing Computational Science Research Center, Beijing 100084, China

ABSTRACT: The adsorption of atoms is one of the efficient approaches for functionalizing two-dimensional (2D) layer materials with desirable properties. The structural knowledge of atoms adsorbed on 2D layer materials is crucial for understanding their functional performance. Here we propose a versatile method for predicting the structures of atoms adsorbed on 2D materials via the swarm-intelligence-based CALYPSO structure-prediction method. Several techniques are implemented to improve the efficiency of structure searching, including fixed adsorption sites, constraints of symmetry and distance during structure generation, and the constrained particle swarm-optimization algorithm for structure evolution. The method is successfully applied to investigate the well-studied systems of hydrogenated and oxidized graphene. The energetically most stable structures of single-sided hydrogenated graphene are predicted for different contents of hydrogen; altering the hydrogen content appears to effectively tune the band gap. An energetically most stable phase of fully oxidized graphene is also uncovered. These results provide new structural knowledge on the adsorption of atoms on graphene.

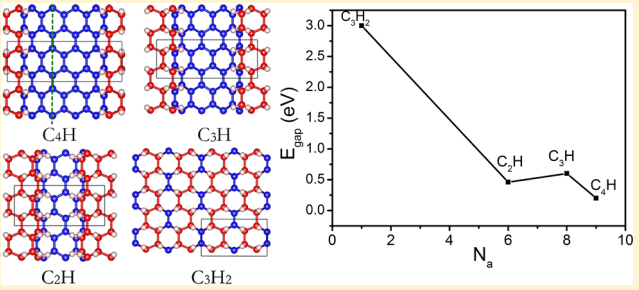

I. INTRODUCTION

Two-dimensional (2D) materials have received much attention owing to their novel electronic and structural properties, which are dramatically different from those of their three-dimensional counterparts.[1,2] The industrial applicability of pristine 2D materials is limited by their specific properties, but the chemical or physical adsorption of atoms, molecules, or functional groups on such materials can effectively modify their properties (e.g., band gap, electron mobility, and magnetism). Important examples include atoms such as H, F, and O adsorbed on graphene to provide a suitable band gap for transistor applications.[3−7] Moreover, atoms adsorbed on 2D materials are potentially useful for ion batteries,[8] hydrogen storage materials,[9] and superconductors.[10]

The physical and chemical properties of a material depend on its specific structure. While several techniques (e.g., scanning tunneling microscopy[3] and Raman spectroscopy[11]) can be used to study the structures of atoms adsorbed on 2D materials, structures often remain experimentally unsolvable[11,12] due to technical limitations. The alternative of solving structures by theoretical methods uses models built manually or obtained from molecular dynamics simulations.[13−16] These methods are efficient particularly when there are few adsorbed atoms where the number of structure variants is relatively small. However, increasing the number of adsorbed atoms rapidly increases the number of possible configurations, which makes these theoretical methods difficult to apply and requires sophisticated users. There is a general request to seek for more efficient structure searching methods able to predict reliably the structure configuration of adatoms without priori structural knowledge. However, only a few efforts have been attempted to develop such methods.[17]

Atomistic structure prediction techniques have been developed[18−26] and widely applied to many important structural problems.[27−29] We developed CALYPSO (Crystal structure AnaLYsis by Particle Swarm Optimization) for structure prediction.[18,30] This method can efficiently explore the multidimensional potential-energy surface, and it requires no prior structure information except the chemical composition. It is designed to predict the structure for 3D crystals,[18] isolated clusters or molecules,[31] surface reconstructions,[32] 2D layer materials,[33] and searching of functional materials (e.g., superhard material)[34] and has been successfully applied to many important systems (e.g., semiconducting lithium,[35] B_{38} clusters,[36] and the diamond surface[32]).

Here we report a generalized CALYPSO method to predict the structures of atoms adsorbed on 2D layered materials. It implements specific structure-searching techniques for this purpose, including using fixed adsorption sites, symmetry and minimal interatomic distance constraints, and a constrained particle swarm-optimization algorithm. The developed method is benchmarked using two typical systems (hydrogenated and oxidized graphene), successfully reproducing their known stable structures. Besides, our study uncovers two new, unexpected,

Received: May 27, 2015
Revised: July 13, 2015
Published: August 3, 2015

DOI: 10.1021/acs.jpcc.5b05035
J. Phys. Chem. C 2015, 119, 20111−20118

low-energy structures of fully hydrogenated graphene. The energetically most stable structures are predicted for single-sided hydrogenated graphene with various contents of hydrogen, where band gaps can be tuned by changing the widths of nanoroads in these stable structures. Furthermore, our method reveals the energetically best structure reported thus far for oxidized graphene.

The remaining sections of this paper are organized as follows. In section II, the method and its implementation are discussed in detail. Applications of the method on hydrogenated and oxidized graphene are described in section III. Finally, a summary is provided in section IV.

II. METHOD AND IMPLEMENTATION

We developed an automatic structure prediction method for atoms adsorbed on 2D layers; it comprises the four main steps depicted in the flowchart in Figure 1. First, initial structures are randomly generated with symmetry constraints. Then, the symmetry function[33,37,38] for fingerprinting structures is calculated to examine the similarity of a given structure with all the previous ones. If the distance metric shows that the newly generated structure is similar to the previous ones, it is discarded. After all the structures of each population are generated, variable-cell geometry optimizations are performed to produce physically justified structures sitting at the local minima of the potential energy surface. Finally, energy surface minimization is performed by the particle swarm optimization (PSO) algorithm,[18,39] which in practice is adopted to update the structures for the next generation. To enhance structural diversity, unbiased structure generation, and coverage of the entire configuration space, a changeable amount of random structures (typically 40%) is created and included in each structure generation calculation.

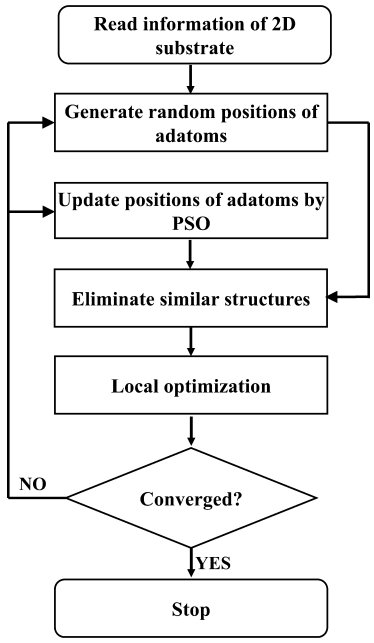

Figure 1. Flowchart of the CALYPSO code for the structure prediction of atoms adsorbed on 2D layered materials.

The structures of atoms adsorbed on each 2D layer are simulated using a slab, which typically consists of two regions: the substrate and the adsorbed region. Atoms in the substrate are fixed so as to preserve its 2D nature, while atoms in the adsorbed region are subjected to swarm evolution. The adsorbed atoms can generally occupy any position in the adsorbed region, but in some particular cases they are known to stay at specific positions on the substrate. For example, hydrogen adsorbed on graphene is known to sit at the top sites above the carbon atoms,[3,40] while oxygen atoms occupy the bridge sites at the midpoints of carbon−carbon bonds.[41] Thus, two structure searching modules including unfixed adsorption sits (UAS) and fixed adsorption sites (FAS) have been implemented in CALYPSO. The UAS module should be used for systems lacking prior knowledge of the adsorption sites. But for systems where atoms are known to adsorb on specific positions, generating the structures with FAS technique is highly efficient since it significantly reduces the search space and generates physically justified structures. Consider the example of 100 structures generated for hydrogenated graphene at four different H coverages (C_6H, C_3H, C_2H, and C_3H_2) using each module. The results (Figure 2a) show that, with increasing H contents, the proportion of reasonable structures generated with UAS module decreases rapidly. For the highest hydrogen coverage (C_3H_2) the FAS module produces 96%

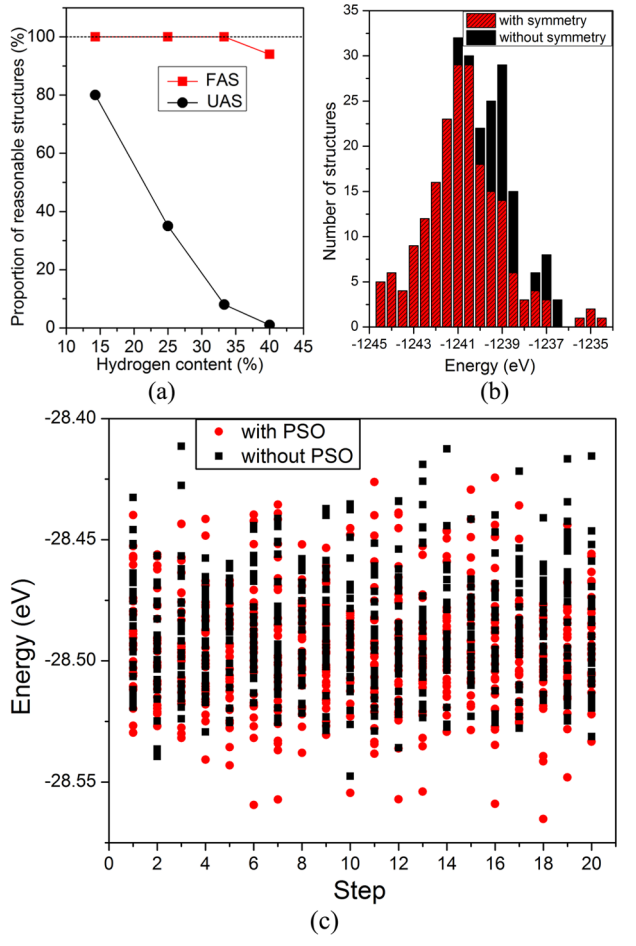

Figure 2. (a) Proportion of reasonable structures generated using adsorption sites that are fixed (FAS, solid squares) or unfixed (UAS, solid circles). (b) Energetic distributions of randomly generated structures with or without symmetry constraints for semihydrogenated graphene. (c) History of a CALYPSO structure search performed on fully hydrogenated graphene with 60% structures updated with PSO (red circles) or without PSO (black squares).

DOI: 10.1021/acs.jpcc.5b05035
J. Phys. Chem. C 2015, 119, 20111−20118

reasonable structures, while only 1% of those generated by the UAS module are reasonable.

We employ symmetry constraints (Figure 3) to generate the random structures.[15,24−26] For a 2D layer, there are only four

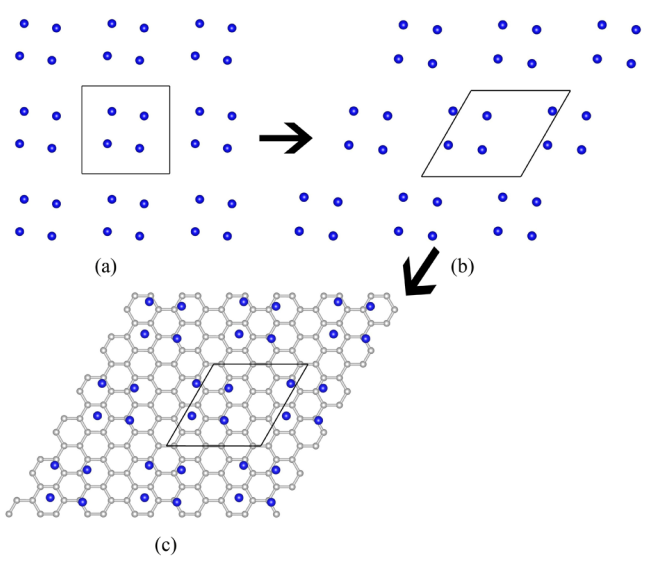

Figure 3. Representation of structure generation with symmetry constraints. (a) The lattice and the positions of adatoms (indicated by blue balls) are generated based on a randomly selected space group. (b) The lattice and adatom positions are transformed to match the crystallographic system of the 2D substrate shown in (c). (c) The transformed adatoms are placed on the 2D substrate indicated by gray balls. The solid line indicates the unit cell.

different crystallographic systems (oblique, rectangular, square, and hexagonal) with 17 planar space groups instead of the 230 space groups for a 3D bulk material. We randomly select a plane space group, and create an adsorption lattice of equal area to the 2D substrate. The positions of the adatoms are generated based on the Wyckoff positions matching the chosen space group (Figure 3a). If the crystallographic system of the current lattice is not the same as that of the 2D substrate, it has to be transformed into the same system. Similarly, the coordinations of adatoms need to be transformed (Figure 3b,c). Note that symmetry constraints on structure generation play a critical role in enhancing structural diversity and generating physically justified structures. Consider semihydrogenated graphene as an example. A supercell containing 24 carbon atoms and 12 hydrogen atoms is selected, and 100 structures are randomly generated with and without symmetry constraints. After structural optimization using Density-Functional-based Tight Binding (DFTB+),[42] the obtained energetic distributions of the structures are shown in Figure 2b. It is seen that the structures generated with symmetry constraints are distributed over a larger energy range and show a higher structural diversity than those randomly sampled. More importantly, constrained structure generation produces many low-energy structures: about 15% were of low energy (−1244.5 to −1243.5 eV). In contrast, no low-energy structures are generated without the constraints (Figure 2b). This example clearly demonstrates that symmetry constraints on structure generation improve the efficiency of structure searching.

Applying a minimal interatomic distance is another constraint on structure generation and has previously been applied to the structure prediction of 2D surface reconstruction[32] and 3D crystals,[18,30] proving to be efficient in eliminating unphysical structures, especially for large systems. The current implementation classifies the interatomic distances into two categories: those between adatoms and substrate atoms, and those between adatoms. Here we restrict the coordinates of adatoms along the direction perpendicular to the 2D plane of the substrate to ensure their sufficient separation from the substrate atoms.

To fingerprint the structures of atoms adsorbed on 2D materials, a set of symmetry functions are adopted in our method. Detailed equations and the properties of the functions can be found in ref 43. The reliability of the fingerprinting method for 2D structures has been demonstrated in our previous study.[33] For each atom, we use 33 different symmetry functions containing information on bond lengths and angles to characterize the atomic environment. The similarity between two structures is thus given by the difference of their atomic symmetry functions.

The local PSO algorithm[18,39] is adopted for energy surface minimization. Here a structure in the search space is represented as a particle, and a set of particles is called a generation. Structures are evolved by the PSO formula:

$$x_i^{t+1} = x_i^t + v_i^{t+1} \tag{1}$$

where i and t are the index of the structure and of the generation, respectively; and x and v represent the positions and velocities of the structure, respectively. They are N-dimensional vectors relating to the degrees of freedom of atomic positions, where N is the number of adatoms in the simulation cell. Note that the atoms in the substrate region are fixed, and only the positions of the adatoms need to be updated. Therefore, the structural positions can be represented by the positions of the adatoms, while the structural velocities represent the variations of the positions of the adatoms. The velocities v of the structures in the first generation are generated randomly. The velocities v_i^{t+1} of the structures in the next generation are calculated as follows:

$$v_i^{t+1} = \omega v_i^t + c_1 r_1(\mathrm{pbest}_i^t - x_i^t) + c_2 r_2(\mathrm{lbest}_i^t - x_i^t) \tag{2}$$

where pbest_i^t is the ith optimized structure, lbest_i^t is the low-energy structure nearest to the ith structure evaluated by symmetry functions, ω is the inertia weight in the range of 0.4−0.9, $c_1 = c_2 = 2$, and r_1 and r_2 are two random numbers uniformly distributed in the range $[0,1]$.

A modified constrained PSO is developed for the FAS module. In most cases, the adatoms generated by PSO may not occupy exactly the given adsorption sites. In such a case, the PSO velocities of the structures in the next generation are adjusted to constrain the adatoms to sit on their nearest adsorption sites. We test the efficiency of the constrained PSO algorithm, taking a fully hydrogenated graphene unit cell of 32 carbon atoms and 32 hydrogen atoms as an example. Two different structure prediction runs are compared: one selects the 60% of structures with low energy to produce by PSO the structures in the next generation, and the other randomly generates all the structures in the next generation (i.e., without PSO). The results (Figure 2c) show that structures generated by constrained PSO are distributed in lower-energy regions than those generated randomly, clearly demonstrating that the constrained PSO algorithm can significantly improve the structure searching efficiency. It should be emphasized that PSO plays a critical role in structure evolution to find the global

DOI: 10.1021/acs.jpcc.5b05035
J. Phys. Chem. C 2015, 119, 20111−20118

stable structure. Here, the energetically stable structure is indeed generated by the constrained PSO.

III. APPLICATIONS AND RESULTS

All techniques described in section II have been implemented into the CALYPSO code. Here, we apply it to investigate two typical adsorbed systems: hydrogenated and oxided graphene. DFTB+ and Vienna Ab initio Simulation Package (VASP)[44] are respectively adopted for local optimizations of the two systems' structures. The DFTB calculations use a k-spacing of 0.37 $Å^{-1}$ in reciprocal space to ensure good convergence of energy. In the VASP calculations, we use projector-augmented wave potentials[45] to describe the core electrons. The energy evaluations use the generalized gradient approximation (GGA) of Perdew, Burke, and Ernzernhof (PBE)[46] for hydrogenated graphene and the local density approximation (LDA)[47] for oxidized graphene with cutoff energies of 500 and 750 eV, respectively. The k-spacings are set to 0.15 $Å^{-1}$ in reciprocal space. All the energy calculations converge to less than 1 meV/atom. The effective masses of the predicted structures are calculated using BoltzTraP.[48]

To reduce the constraints imposed by periodicity, supercells of different sizes are used. For both-sided fully hydrogenated graphene (graphane), we use 1 × 4 and 2 × 2 supercells for C_8H_8, a $(\sqrt{3} \times 2\sqrt{3})R30°$ supercell for $C_{12}H_{12}$, $(\sqrt{3} \times 4\sqrt{3})R30°$ and $(\sqrt{3} \times 2\sqrt{3})R30°$ supercells for $C_{24}H_{24}$, and a 4 × 4 supercell for $C_{32}H_{32}$. Two rectangular supercells accommodating C_8H_8 and $C_{16}H_{16}$ are also considered. Partially hydrogenated single-sided graphene is modeled using a 4 × 4 supercell to accommodate $C_{32}H_8$. A rectangular supercell and a $(\sqrt{3} \times 4\sqrt{3})R30°$ supercell are used to accommodate $C_{24}H_6$, $C_{24}H_8$, $C_{24}H_{12}$, and $C_{24}H_{16}$. For oxidized graphene, we use a $(\sqrt{3} \times 2\sqrt{3})R30°$ supercell to accommodate $C_{12}O_{12}$. The dynamic stabilities of all the predicted structures are examined by first-principles molecular dynamics simulations with a 0.5 fs time step. All structures remain almost intact at 1000 K after running 2000 molecular dynamic steps.

A. Hydrogenated Graphene. Graphene has attracted considerable attention owing to its potential applicability in emerging areas such as electronic devices.[2−4,49] However, its zero band gap limits its application in electronic devices. Hydrogenation can functionalize graphene sheets to provide an open band gap.[3,5,50,51] The level of hydrogen coverage can lead to fully hydrogenated graphene, referred as graphane, or partially hydrogenated graphene. Graphane has been proposed theoretically to show several structures,[13,52] but all graphane conformers have large band gaps of about 3.5 eV,[53] making them unsuitable for electronic applications. Previous studies have shown that varying the degree of hydrogen coverage of partially hydrogenated graphene can effectively tune its band gap.[3,5,50,51] For example, single-side hydrogenated graphene has a band gap of 0.43 eV,[54] and a single hydrogen atom in a 32-carbon-atom slab creates a gap of about 1.25 eV.[55] We choose graphane here as a benchmark system for our method owing to its possibility of existing as various conformers. We further investigate the stable structures of partially hydrogenated graphene in an effort to tune the band gap by varying hydrogen coverage.

Our CALYPSO method successfully reproduces known structures of graphane, including the chair,[52] tricycle,[56] stirrup,[57] boat-1,[52] and boat-2[13] conformers, validating our approach for predicting the structures of atoms adsorbed on 2D layers. It also reveals two new low-energy structures: the stair (Figure 4c) and the zipper (Figure 4d). Although their energies

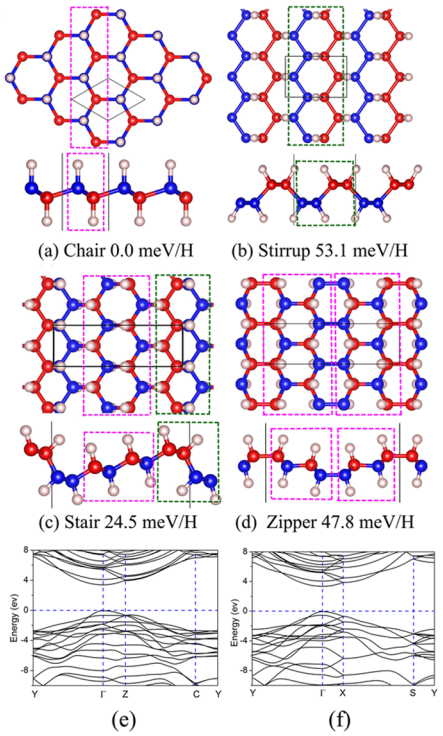

Figure 4. Top view (top panel) and side view (bottom panel) of graphane with (a) chair and (b) stirrup conformers, and the (c) stair and (d) zipper conformers. Energy relative to the chair conformer of each structure is labeled. Red and blue balls represent the carbon atoms with up and down hydrogenation, respectively. The pink balls represent hydrogen atoms, and the solid black line indicates the unit cell. The dashed pink and green lines represent the units with chair and stirrup configurations, respectively. Also shown are band structures of (e) stair and (f) zipper conformers.

are higher than those of the chair (Figure 4a) and tricycle conformers, they are more stable than the stirrup (Figure 4b) and both boat conformers. The atomic arrangement of the stair structure is similar to that of the tricycle structure in that they both contain the chair and stirrup conformer units. The zipper structure contains two normal and two reversed chair chains in one unit cell.

We use PBE to calculate the band structures of the stair and zipper conformers (Figure 4e and f): both show a direct band gap of ∼3.3 eV at the Γ point, and have a large dispersion of the highest valence band along the Γ−Y direction. The hole effective masses of the stair and zipper are $0.26m_0$ (where m_0 is the static mass of one electron) and $0.29m_0$, respectively, along the Γ−Y direction, and $0.87m_0$ along the Γ−Z direction for the stair, and $0.73m_0$ along the Γ−X direction for the zipper. Both structures exhibit distinct anisotropy, unlike the isotropic chair conformer (effective hole mass ∼ $0.46m_0$). Note that PBE is well-known to underestimate band gaps, suggesting that the band gaps of the stair and zipper conformers are in reality much larger than those calculated, thus precluding these new conformers from applications in electronic devices despite their small effective masses along the Γ−Y direction.

We next explore the stable structures of partially single-sided hydrogenated graphene for high hydrogen contents of C_4H, C_3H, C_2H, and C_3H_2. The lowest-energy structures discovered

DOI: 10.1021/acs.jpcc.5b05035
J. Phys. Chem. C 2015, 119, 20111−20118

by CALYPSO in each case are shown in Figure 5. Note that our C_4H structure has much lower formation energy (by 0.19 eV/H) than the lowest-energy structure[58] built manually. Similarly, our C_2H structure has a formation energy much lower (by 1.01 eV/H) than the earlier best structure (referred as graphone).[59] Our predicted structures of the partially hydrogenated graphene sheets of C_4H (Figure 5a), C_3H (Figure 5b), C_2H (Figure 5c), and C_3H_2 (Figure 5d) show two regions: hydrogenated substrate and pristine graphene. The hydrogenated region separates the pristine graphene, patterning graphene nanoroads, as proposed by Singh et al.[5] in both-sided hydrogenated graphene. Varying the degree of hydrogenation alters the widths of the nanoroads as measured by sp^2-carbon dimer lines. Specially, there are 9, 8, 6, and 1 sp^2-carbon dimer lines in the structures of C_4H, C_3H, C_2H, and C_3H_2, respectively.

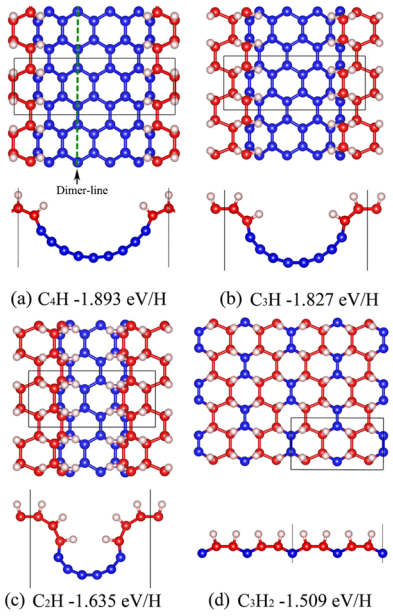

Figure 5. (a–d) Top view (top panel) and side view (bottom panel) of the lowest-energy structures of C_4H, C_3H, C_2H, and C_3H_2, respectively. Solid black line indicates the unit cell. Red and blue balls represent hydrogenated and bare carbon atoms, respectively. Dashed green line in (a) indicates an sp^2-carbon dimer line. Pink balls represent hydrogen atoms. The formation energy of each structure is given below the pictures, and is defined as $E_{form} = E(C_xH) - xE(C) - E(H)$, where $E(C)$ is the energy of graphene per carbon and $E(H)$ is the energy of a single H atom.

The band gap can be tuned by varying the widths of the embedded nanoroads, as shown in Figure 6e. Increasing hydrogen coverage constricts the nanoroads, and the band gap increases from 0.4 to 3.0 eV. Our results thus demonstrate that changing the hydrogen coverage on single-sided hydrogenated graphene can efficiently tune its band gap.

We calculated the band structures (Figure 6a–d) of these structures using PBE. Note that C_4H (Figure 6a), C_3H (Figure 6b), and C_2H (Figure 6c) have similar band structures besides C_3H_2 (Figure 6d). The valence-band maxima (VBM) and conduction-band minima (CBM) of C_4H, C_3H, and C_2H along the $\Gamma-Y$ direction (the left-to-right direction in Figure 5) are almost nondispersive, but exhibit strong dispersion along the $\Gamma-X$ or $Y-S$ direction (the top-to-bottom direction in Figure 5), indicating their distinct anisotropic character. The calculated effective masses are listed in Table 1; those along the $\Gamma-X$ or $Y-S$ direction associating with sp^2-carbon dimer lines are relatively small. Note that the magnitudes of the effective masses of structures of C_4H, C_3H, and C_2H with small band gap are comparable to those of zincblende GaN,[60] suggesting that these structures can be used for electronic devices with significant anisotropic behavior.

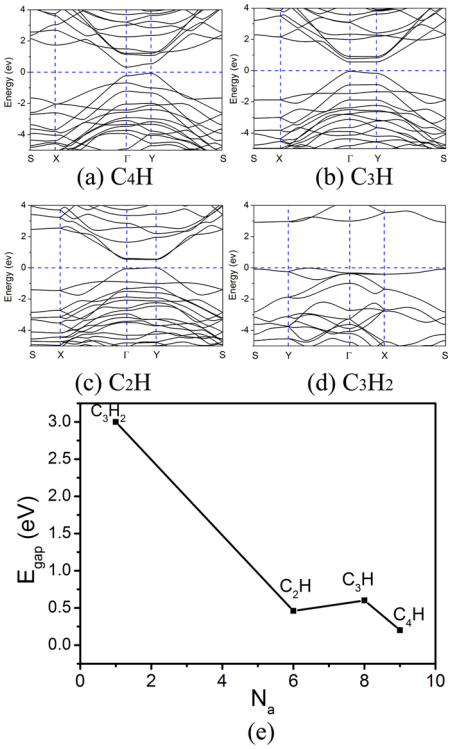

Figure 6. (a–d) Band structures of the lowest-energy structures of C_4H, C_3H, C_2H, and C_3H_2, respectively. (e) Variation in band gap with the number of sp^2-carbon dimer-lines (N_a) in the partially single-sided hydrogenated graphene.

Table 1. Effective Masses of Predicted Structures of C_4H, C_3H, C_2H, and C_3H_2[a]

	$\Gamma-Y$ direction		$\Gamma-X$ or $Y-S$ direction	
	m_e	m_h	m_e	m_h
C_4H	$0.61m_0$	$0.80m_0$	$0.09m_0$	$0.09m_0$
C_3H	$320.93m_0$	$1.469m_0$	$0.15m_0$	$0.13m_0$
C_2H	$74.17m_0$	$5.75m_0$	$0.16m_0$	$0.13m_0$
C_3H_2	$16.43m_0$	$3.50m_0$	$0.74m_0$	$1.30m_0$

[a] m_e and m_h are the effective masses of an electron and a hole, respectively. m_0 is the static mass of one electron.

B. Oxidized Graphene. Oxidized graphene is a promising precursor for the mass production of graphene via a solution-based chemical reduction route.[61,62] Graphene monoxide (GMO) with a 1:1 stoichiometric ratio of C and O has been synthesized,[12] but its exact structure remains unknown. Several low-energy structures have been proposed theoretically.[17,63] Two low-energy ordered structures, the mix model and the epoxy pair model, have been predicted via structure searches based on the genetic algorithm,[17] and the mix model has a lower energy than epoxy pair model. Two energetically more favorable structures, named z-GMO and a-GMO, were later proposed,[63] but these structures have substantial deviation from the structural features of graphene. The two structures are therefore not discussed or compared below.

DOI: 10.1021/acs.jpcc.5b05035
J. Phys. Chem. C 2015, 119, 20111–20118

We used our method to investigate the structures of GMO. The mix model and epoxy pair model were successfully reproduced, validating our approach. Besides, we predicted a novel structure (Figure 7a) referred to as central-symmetric mix

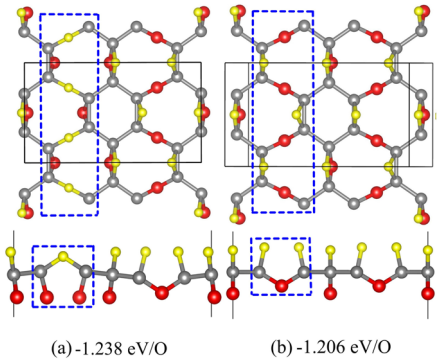

Figure 7. Top view (top panel) and side view (bottom panel) of (a) the central-symmetric mix model predicted by CALYPSO and (b) the mix model from ref 17. Gray and red balls represent carbon and oxygen atoms below the layer, respectively, and yellow balls indicate oxygen atoms above the layer. Solid black line indicates the unit cell. The dashed blue line represents the upside-down region. The formation energy of each structure is given below the pictures, and is defined as $E_{form} = E(C_xO) - xE(C) - E(O)$, where $E(C)$ is the energy of graphene per carbon atom and $E(O) = 1/2E(O_2)$.

structure (D_{2h} symmetry). Our calculations demonstrated that our new structure is energetically more stable than mix-model (Figure 7b) by 32 meV/O. The central-symmetric mix structure might be seen as turning over half normal and unzipped epoxy groups shown in the region enclosed by the dashed blue line in Figure 7b of the mix model. The normal and unzipped epoxy groups are distributed on both sides of the graphene sheet.

IV. CONCLUSION

An efficient method for predicting the structures of atoms adsorbed on 2D layers is developed and implemented in the CALYPSO software package. Several especially designed techniques, including FAS, symmetry and minimal distance constraints, and a constrained PSO algorithm, are introduced to improve the structure searching efficiency. Our method is benchmarked and applied to the well-studied systems of fully and partially hydrogenated graphene and graphene oxide. The known phases of graphane are readily reproduced, and two new low-energy structures are predicted. The energetically most stable structures of single-sided hydrogenated graphene with various amounts of hydrogen are predicted, and the band gap appears to be tuned by the changing widths of nanoroads in these stable structures. Our method predicts the energetically best structure yet reported for oxidized graphene. In general, our method is a promising approach for the smart prediction and design of structures of atoms adsorbed on 2D layered materials. Furthermore, it can be applied to the structure prediction of atoms adsorbed on surfaces by switching the substrate to a predefined surface other than one layer and then applying the major techniques as used here.

AUTHOR INFORMATION

Corresponding Authors

*E-mail: wyc@calypso.cn (Y.W.).

*E-mail: mym@jlu.edu.cn (Y.M.).

Notes

The authors declare no competing financial interest.

ACKNOWLEDGMENTS

This work was supported by the 973 Program (Grant No. 2011CB808200), the NSF of China (Grant Nos. 11274136 and 11404128), and the 2012 Changjiang Scholars Program of China. Computation was carried out at the High Performance Computing Center of Jilin University.

REFERENCES

(1) Novoselov, K. S. Electric Field Effect in Atomically Thin Carbon Films. *Science* **2004**, *306*, 666−669.
(2) Novoselov, K. S.; Geim, A. K.; Morozov, S. V.; Jiang, D.; Katsnelson, M. I.; Grigorieva, I. V.; Dubonos, S. V.; Firsov, A. A. Two-Dimensional Gas of Massless Dirac Fermions in Graphene. *Nature* **2005**, *438*, 197−200.
(3) Balog, R.; Jørgensen, B.; Nilsson, L.; Andersen, M.; Rienks, E.; Bianchi, M.; Fanetti, M.; Lægsgaard, E.; Baraldi, A.; Lizzit, S.; et al. Bandgap Opening in Graphene Induced by Patterned Hydrogen Adsorption. *Nat. Mater.* **2010**, *9*, 315−319.
(4) Gilje, S.; Han, S.; Wang, M.; Wang, K. L.; Kaner, R. B. A Chemical Route to Graphene for Device Applications. *Nano Lett.* **2007**, *7*, 3394−3398.
(5) Singh, A. K.; Yakobson, B. I. Electronics and Magnetism of Patterned Graphene Nanoroads. *Nano Lett.* **2009**, *9*, 1540−1543.
(6) Li, Y.; Pantoja, B. A.; Chen, Z. Self-Modulated Band Structure Engineering in C_4F Nanosheets: First-Principles Insights. *J. Chem. Theory Comput.* **2014**, *10*, 1265−1271.
(7) Garay-Tapia, A. M.; Romero, A. H.; Barone, V. Lithium Adsorption on Graphene: From Isolated Adatoms to Metallic Sheets. *J. Chem. Theory Comput.* **2012**, *8*, 1064−1071.
(8) Liu, Y.; Wang, Y. M.; Yakobson, B. I.; Wood, B. C. Assessing Carbon-Based Anodes for Lithium-Ion Batteries: A Universal Description of Charge-Transfer Binding. *Phys. Rev. Lett.* **2014**, *113*, 028304.
(9) Lin, Y.; Ding, F.; Yakobson, B. I. Hydrogen Storage by Spillover on Graphene as a Phase Nucleation Process. *Phys. Rev. B: Condens. Matter Mater. Phys.* **2008**, *78*, 041402.
(10) Yang, S.-L.; Sobota, J. A.; Howard, C. A.; Pickard, C. J.; Hashimoto, M.; Lu, D. H.; Mo, S.-K.; Kirchmann, P. S.; Shen, Z.-X. Superconducting Graphene Sheets in CaC_6 Enabled by Phonon-Mediated Interband Interactions. *Nat. Commun.* **2014**, *5*, 3493.
(11) Elias, D. C.; Nair, R. R.; Mohiuddin, T. M. G.; Morozov, S. V.; Blake, P.; Halsall, M. P.; Ferrari, A. C.; Boukhvalov, D. W.; Katsnelson, M. I.; Geim, A. K. Control of Graphene's Properties by Reversible Hydrogenation: Evidence for Graphane. *Science* **2009**, *323*, 610−613.
(12) Mattson, E. C.; Pu, H.; Cui, S.; Schofield, M. A.; Rhim, S.; Lu, G.; Nasse, M. J.; Ruoff, R. S.; Weinert, M.; Gajdardziska-Josifovska, M.; et al. Evidence of Nanocrystalline Semiconducting Graphene Monoxide during Thermal Reduction of Graphene Oxide in Vacuum. *ACS Nano* **2011**, *5*, 9710−9717.
(13) Leenaerts, O.; Peelaers, H.; Hernández-Nieves, A. D.; Partoens, B.; Peeters, F. M. First-Principles Investigation of Graphene Fluoride and Graphane. *Phys. Rev. B: Condens. Matter Mater. Phys.* **2010**, *82*, 195436.
(14) Flores, M. Z. S.; Autreto, P. A. S.; Legoas, S. B.; Galvao, D. S. Graphene to Graphane: A Theoretical Study. *Nanotechnology* **2009**, *20*, 465704.
(15) Dzhurakhalov, A. A.; Peeters, F. M. Structure and Energetics of Hydrogen Chemisorbed on a Single Graphene Layer to Produce Graphane. *Carbon* **2011**, *49*, 3258−3266.
(16) Liu, H. Y.; Hou, Z. F.; Hu, C. H.; Yang, Y.; Zhu, Z. Z. Electronic and Magnetic Properties of Fluorinated Graphene with Different Coverage of Fluorine. *J. Phys. Chem. C* **2012**, *116*, 18193−18201.

DOI: 10.1021/acs.jpcc.5b05035
J. Phys. Chem. C 2015, 119, 20111−20118

(17) Xiang, H. J.; Wei, S.-H.; Gong, X. G. Structural Motifs in Oxidized Graphene: A Genetic Algorithm Study Based on Density Functional Theory. *Phys. Rev. B: Condens. Matter Mater. Phys.* **2010**, *82*, 035416.
(18) Wang, Y.; Lv, J.; Zhu, L.; Ma, Y. Crystal Structure Prediction via Particle-Swarm Optimization. *Phys. Rev. B: Condens. Matter Mater. Phys.* **2010**, *82*, 094116.
(19) Meredig, B.; Wolverton, C. A Hybrid Computational–experimental Approach for Automated Crystal Structure Solution. *Nat. Mater.* **2012**, *12*, 123–127.
(20) Glass, C. W.; Oganov, A. R.; Hansen, N. USPEX—Evolutionary Crystal Structure Prediction. *Comput. Phys. Commun.* **2006**, *175*, 713–720.
(21) Trimarchi, G.; Zunger, A. Global Space-Group Optimization Problem: Finding the Stablest Crystal Structure without Constraints. *Phys. Rev. B: Condens. Matter Mater. Phys.* **2007**, *75*, 104113.
(22) Pickard, C. J.; Needs, R. J. *Ab Initio* Random Structure Searching. *J. Phys.: Condens. Matter* **2011**, *23*, 053201.
(23) Lonie, D. C.; Zurek, E. XtalOpt: An Open-Source Evolutionary Algorithm for Crystal Structure Prediction. *Comput. Phys. Commun.* **2011**, *182*, 372–387.
(24) Liu, Z.-L. Muse: Multi-Algorithm Collaborative Crystal Structure Prediction. *Comput. Phys. Commun.* **2014**, *185*, 1893–1900.
(25) Wu, S. Q.; Ji, M.; Wang, C. Z.; Nguyen, M. C.; Zhao, X.; Umemoto, K.; Wentzcovitch, R. M.; Ho, K. M. An Adaptive Genetic Algorithm for Crystal Structure Prediction. *J. Phys.: Condens. Matter* **2014**, *26*, 035402.
(26) Wang, Y.; Ma, Y. Perspective: Crystal Structure Prediction at High Pressures. *J. Chem. Phys.* **2014**, *140*, 040901.
(27) Zhu, L.; Liu, H.; Pickard, C. J.; Zou, G.; Ma, Y. Reactions of Xenon with Iron and Nickel Are Predicted in the Earth's Inner Core. *Nat. Chem.* **2014**, *6*, 644–649.
(28) Wang, Q.; Oganov, A. R.; Zhu, Q.; Zhou, X.-F. New Reconstructions of the (110) Surface of Rutile TiO_2 Predicted by an Evolutionary Method. *Phys. Rev. Lett.* **2014**, *113*, 266101.
(29) Nicholls, R. J.; Ni, N.; Lozano-Perez, S.; London, A.; McComb, D. W.; Nellist, P. D.; Grovenor, C. R. M.; Pickard, C. J.; Yates, J. R. Crystal Structure of the ZrO Phase at Zirconium/Zirconium Oxide Interfaces. *Adv. Eng. Mater.* **2015**, *17*, 211–215.
(30) Wang, Y.; Lv, J.; Zhu, L.; Ma, Y. CALYPSO: A Method for Crystal Structure Prediction. *Comput. Phys. Commun.* **2012**, *183*, 2063–2070.
(31) Lv, J.; Wang, Y.; Zhu, L.; Ma, Y. Particle-Swarm Structure Prediction on Clusters. *J. Chem. Phys.* **2012**, *137*, 084104.
(32) Lu, S.; Wang, Y.; Liu, H.; Miao, M.; Ma, Y. Self-Assembled Ultrathin Nanotubes on Diamond (100) Surface. *Nat. Commun.* **2014**, *5*, 3666.
(33) Wang, Y.; Miao, M.; Lv, J.; Zhu, L.; Yin, K.; Liu, H.; Ma, Y. An Effective Structure Prediction Method for Layered Materials Based on 2D Particle Swarm Optimization Algorithm. *J. Chem. Phys.* **2012**, *137*, 224108.
(34) Zhang, X.; Wang, Y.; Lv, J.; Zhu, C.; Li, Q.; Zhang, M.; Li, Q.; Ma, Y. First-Principles Structural Design of Superhard Materials. *J. Chem. Phys.* **2013**, *138*, 114101.
(35) Lv, J.; Wang, Y.; Zhu, L.; Ma, Y. Predicted Novel High-Pressure Phases of Lithium. *Phys. Rev. Lett.* **2011**, *106*, 015503.
(36) Lv, J.; Wang, Y.; Zhu, L.; Ma, Y. B_{38}: An All-Boron Fullerene Analogue. *Nanoscale* **2014**, *6*, 11692–11696.
(37) Behler, J.; Parrinello, M. Generalized Neural-Network Representation of High-Dimensional Potential-Energy Surfaces. *Phys. Rev. Lett.* **2007**, *98*, 146401.
(38) Behler, J.; Martoňák, R.; Donadio, D.; Parrinello, M. Metadynamics Simulations of the High-Pressure Phases of Silicon Employing a High-Dimensional Neural Network Potential. *Phys. Rev. Lett.* **2008**, *100*, 185501.
(39) Call, S. T.; Zubarev, D. Y.; Boldyrev, A. I. Global Minimum Structure Searches via Particle Swarm Optimization. *J. Comput. Chem.* **2007**, *28*, 1177–1186.
(40) Boukhvalov, D.; Katsnelson, M.; Lichtenstein, A. Hydrogen on Graphene: Electronic Structure, Total Energy, Structural Distortions and Magnetism from First-Principles Calculations. *Phys. Rev. B: Condens. Matter Mater. Phys.* **2008**, *77*, 035427.
(41) Yan, J.-A.; Xian, L.; Chou, M. Structural and Electronic Properties of Oxidized Graphene. *Phys. Rev. Lett.* **2009**, *103*, 086802.
(42) Aradi, B.; Hourahine, B.; Frauenheim, T. DFTB+, a Sparse Matrix-Based Implementation of the DFTB Method †. *J. Phys. Chem. A* **2007**, *111*, 5678–5684.
(43) Behler, J. Atom-Centered Symmetry Functions for Constructing High-Dimensional Neural Network Potentials. *J. Chem. Phys.* **2011**, *134*, 074106.
(44) Kresse, G.; Joubert, D. From Ultrasoft Pseudopotentials to the Projector Augmented-Wave Method. *Phys. Rev. B: Condens. Matter Mater. Phys.* **1999**, *59*, 1758–1775.
(45) Blöchl, P. E. Projector Augmented-Wave Method. *Phys. Rev. B: Condens. Matter Mater. Phys.* **1994**, *50*, 17953–17979.
(46) Perdew, J. P.; Burke, K.; Ernzerhof, M. Generalized Gradient Approximation Made Simple. *Phys. Rev. Lett.* **1996**, *77*, 3865–3868.
(47) Perdew, J. P.; Zunger, A. Self-Interaction Correction to Density-Functional Approximations for Many-Electron Systems. *Phys. Rev. B: Condens. Matter Mater. Phys.* **1981**, *23*, 5048–5079.
(48) Madsen, G. K. H.; Singh, D. J. BoltzTraP. A Code for Calculating Band-Structure Dependent Quantities. *Comput. Phys. Commun.* **2006**, *175*, 67–71.
(49) Zhou, S. Y.; Gweon, G.-H.; Fedorov, A. V.; First, P. N.; de Heer, W. A.; Lee, D.-H.; Guinea, F.; Castro Neto, A. H.; Lanzara, A. Substrate-Induced Bandgap Opening in Epitaxial Graphene. *Nat. Mater.* **2007**, *6*, 770–775.
(50) Chernozatonskii, L. A.; Sorokin, P. B.; Brüning, J. W. Two-Dimensional Semiconducting Nanostructures Based on Single Graphene Sheets with Lines of Adsorbed Hydrogen Atoms. *Appl. Phys. Lett.* **2007**, *91*, 183103.
(51) Xiang, H. J.; Kan, E. J.; Wei, S.-H.; Gong, X. G.; Whangbo, M.-H. Thermodynamically Stable Single-Side Hydrogenated Graphene. *Phys. Rev. B: Condens. Matter Mater. Phys.* **2010**, *82*, 165425.
(52) Sofo, J.; Chaudhari, A.; Barber, G. Graphane: A Two-Dimensional Hydrocarbon. *Phys. Rev. B: Condens. Matter Mater. Phys.* **2007**, *75*, 153401.
(53) Zhou, C.; Chen, S.; Lou, J.; Wang, J.; Yang, Q.; Liu, C.; Huang, D.; Zhu, T. Graphene's Cousin: The Present and Future of Graphane. *Nanoscale Res. Lett.* **2014**, *9*, 1–9.
(54) Zhou, J.; Wu, M. M.; Zhou, X.; Sun, Q. Tuning Electronic and Magnetic Properties of Graphene by Surface Modification. *Appl. Phys. Lett.* **2009**, *95*, 103108.
(55) Duplock, E.; Scheffler, M.; Lindan, P. Hallmark of Perfect Graphene. *Phys. Rev. Lett.* **2004**, *92*, 225502.
(56) He, C.; Zhang, C. X.; Sun, L. Z.; Jiao, N.; Zhang, K. W.; Zhong, J. Structure, Stability and Electronic Properties of Tricycle Type Graphane. *Phys. Status Solidi RRL* **2012**, *6*, 427–429.
(57) Bhattacharya, A.; Bhattacharya, S.; Majumder, C.; Das, G. P. Third Conformer of Graphane: A First-Principles Density Functional Theory Study. *Phys. Rev. B: Condens. Matter Mater. Phys.* **2011**, *83*, 033404.
(58) Haberer, D.; Giusca, C. E.; Wang, Y.; Sachdev, H.; Fedorov, A. V.; Farjam, M.; Jafari, S. A.; Vyalikh, D. V.; Usachov, D.; Liu, X.; et al. Evidence for a New Two-Dimensional C_4H-Type Polymer Based on Hydrogenated Graphene. *Adv. Mater.* **2011**, *23*, 4497–4503.
(59) Zhou, J.; Wang, Q.; Sun, Q.; Chen, X. S.; Kawazoe, Y.; Jena, P. Ferromagnetism in Semihydrogenated Graphene Sheet. *Nano Lett.* **2009**, *9*, 3867–3870.
(60) Yu, P. Y.; Cardona, M. *Fundamentals of Semiconductors: Physics and Materials properties*, 3rd ed.; Springer: Berlin, Heidelberg, 2005.
(61) Mkhoyan, K. A.; Contryman, A. W.; Silcox, J.; Stewart, D. A.; Eda, G.; Mattevi, C.; Miller, S.; Chhowalla, M. Atomic and Electronic Structure of Graphene-Oxide. *Nano Lett.* **2009**, *9*, 1058–1063.
(62) Kumar, P. V.; Bardhan, N. M.; Tongay, S.; Wu, J.; Belcher, A. M.; Grossman, J. C. Scalable Enhancement of Graphene Oxide

DOI: 10.1021/acs.jpcc.5b05035
J. Phys. Chem. C 2015, 119, 20111–20118

Properties by Thermally Driven Phase Transformation. *Nat. Chem.* **2013**, *6*, 151−158.
(63) Zhang, S.; Zhou, J.; Wang, Q.; Jena, P. Structure, Stability, and Property Modulations of Stoichiometric Graphene Oxide. *J. Phys. Chem. C* **2013**, *117*, 1064−1070.

DOI: 10.1021/acs.jpcc.5b05035
J. Phys. Chem. C 2015, 119, 20111−20118